Magnetoconductivity in a mesoscopic antidot array

G. M. Sundaram, N. J. Bassom, R. J. Nicholas, and G. J. Rees
Clarendon Laboratory, Parks Road, Oxford OX1 3PU, United Kingdom

P. J. Heard
Oxford Instruments, Eynsham, United Kingdom

P. D. Prewett
Rutherford-Appleton Laboratory, Chilton, Didcot, United Kingdom

J. E. F. Frost and G. A. C. Jones
Cavendish Laboratory, Madingley Road, Cambridge CB3 0HE, United Kingdom

D. C. Peacock
Cavendish Laboratory, Madingley Road, Cambridge CB3 0HE, United Kingdom
and GEC Hirst Research Center, East Lane, Wembley HA9 7PP, United Kingdom

D. A. Ritchie
Cavendish Laboratory, Madingley Road, Cambridge CB3 0HE, United Kingdom
(Received 10 September 1991; revised manuscript received 2 June 1992)

We describe studies of magnetotransport in antidot arrays formed by focused ion-beam implantation. This shows the dominant role played by interconnects between dotlike reservoirs. Two separate Shubnikov–de Haas periodicities are observed at high and low fields, which allow separate measurements of the depth of the reservoirs and the interconnects. A large negative magnetoresistance is observed at low fields, which is interpreted as being due to the formation of propagating edge states as the field increases.

I. INTRODUCTION

There has been intense interest in the study of quantum dot and antidot arrays recently. The majority of work has concentrated on the study of weakly modulated structures[1–4] formed on gated arrays fabricated using electron-beam lithography. These structures have been the basis for the observation of the so-called Weiss oscillations[1–4] in which resonant structure is observed in the magnetoresistance when the classical cyclotron orbit comes into correspondence with the modulating potential. Work on more strongly modulated structures recently has been the basis for the observation of the so-called "pinball" resonances in which carriers make orbits around strong scattering potentials,[5–8] resulting in their being bound to particular orbits containing one or more of the antidot features. Some reports have also been made of structures fabricated using focused ion-beam (FIB) techniques,[8–10] in which patterning is achieved utilizing the modulation of the electron-energy profile by the damage induced in the implantation process.

In this paper we report magnetotransport studies of such FIB structures with a strongly modulating potential. The study of magnetotransport shows us how we can measure both the potential modulation induced by the patterning process and the very large changes in conduction as one goes from a strongly to a weakly interconnected dot array. Optical studies[6] have suggested that coherent orbits interconnecting adjacent dots can be observed, and we demonstrate that these have a dominant influence on the transport properties of the array at high fields.

II. FABRICATION

The starting material for the structures is a single wafer of standard modulation-doped GaAs/$Al_xGa_{1-x}As$ heterojunction grown on a semi-insulating GaAs substrate by molecular-beam epitaxy (MBE). The structure has a spacer layer of 200 Å, a Si-doped $Al_xGa_{1-x}As$ region of 400 Å, and a capping layer of 100 Å. The electron density (N_s) and mobility (μ) at $T=4.2$ K for the sample prior to patterning were $N_s=3.5\times10^{11}$ cm^{-2} and $\mu=6.5\times10^5$ cm^2/Vs. After illumination these values increase to $N_s=4.5\times10^{11}$ cm^{-2} and $\mu=1.2\times10^6$ cm^2/Vs.

A standard Hall bar geometry was lithographically defined on the sample that was subsequently FIB pat-

TABLE I. Sample characteristics.

Sample	V_{ACC} (kV)	I_{beam} (pA)	t_{dwell} (μs)	Spot size (μm)	Period (μm)
1	20	30	1	0.4	1.0
2	10	30	1	0.8	2.0
3	20	30	1	0.4	0.8
4	20	30	1	0.4	1.0
5	42	30	1	0.2	0.8

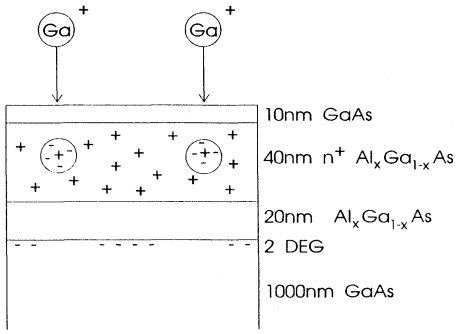

FIG. 1. A schematic view of the sample and focused ion-beam patterning process.

terned to cover the region between the four potential probes. Using an Oxford Instruments Microtrim machine, Ga^+ ions were accelerated and focused to a spot on the samples. A beam current of 30 pA and a dwell time of 1 μs were used to define a square grid of depletion regions on four samples (sample 3, sample 4, sample 1, and sample 2), which have a grid separation of 0.8, 1.0, 1.0, and 2.0 μm, respectively. A fifth sample (sample 5) was coated with ZnS to attenuate the Ga^+ flux, and was patterned with a 0.8-μm grid with an accelerating voltage of 42 keV. A summary of the process parameters is shown in Table I.

The fabricated structures use the idea of damage-induced depletion[8-11] by utilizing the Ga^+ ions to produce damage sites in the semiconductor, which, in turn, act as electron traps. The dose level corresponds to a deposition of $\sim$200 Ga^+ ions per doping point. For the implantation voltages used (10–20 keV) the ions will be channeled down to a depth of order 200–300 Å,[12,13] where negatively charged traps will locally neutralize some of the *n*-type Si doping, as shown in Fig. 1. This creates a two-dimensional (2D) array of depleted regions that consists of an array of wide 2D-electron-gas (2DEG) reservoirs connected by narrow constrictions (an antidot array) as illustrated in Fig. 2, or a quantum dot structure where the interconnects between reservoirs are pinched off by the depleted regions, depending on the strength of the modulating potential. In essence, the FIB process imposes a strong periodic potential that modulates the two-dimensional electron gas. The implantation process creates only electron traps, since the carrier densities after full illumination with visible light are always lower after patterning than in unpatterned samples. It is important to note that the patterning extends beyond the physical edges of the Hall bar and into the potential probes.

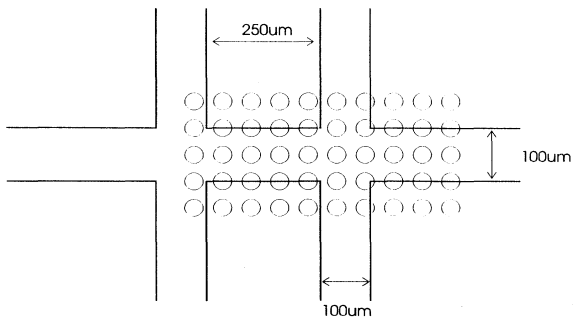

FIG. 2. A schematic view of the Hall bar studied and the extent of the patterned array.

III. EXPERIMENTAL RESULTS

The conductivity and magnetotransport properties of the patterned structures have been studied as a function of carrier density over a wide range using the persistent photoexcitation effect. The shorter period, strongly patterned, structures are close to an array of isolated quantum dots, with the opposite limit of a weak antidot structure being achieved at high carrier densities. Estimates of the sheet carrier density from the high-field magnetotransport described below indicate that the sheet conductivity can vary by a factor of order 10^3 for a threefold increase in carrier density, with radical changes in the carrier conduction process. In an effort to follow the samples through their transition from the strong to the weak connectivity regime (corresponding to a transition from the dot to the antidot picture, where the narrow interconnecting pathways between the 2DEG reservoirs are no longer pinched off, but may act as an array of quantum point contacts), the carrier densities of the structures were increased by progressively illuminating the samples. A magnetoresistance measurement followed each stage of the illumination once the structures began to show a measurable conduction. The magnetotransport measurements were performed using a standard lock-in technique in magnetic fields up to 14.5 T at temperatures of 350 mK and 1.6 K.

Figures 3 and 4 illustrate the gradual change in the nature of the magnetoresistance in sample 4. The traces are characterized by an initially large negative magnetoresistance followed by the emergence of a resistance minimum. As the zero-field resistance decreases, the magnetoresistance develops a clear series of Shubnikov–de Haas (SdH) oscillations that allow us to

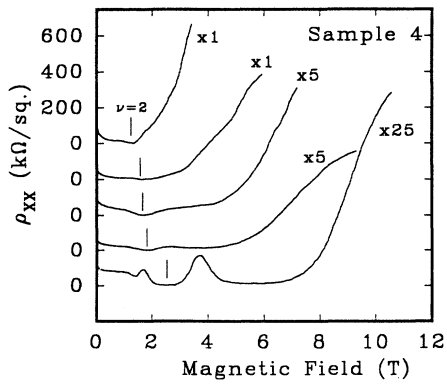

FIG. 3. A series of magnetotransport traces of the conductivity as the electron density is increased by persistent photoexcitation of carriers into sample 4 at 0.35 K.

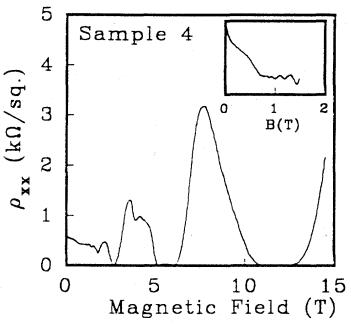

FIG. 4. The high-electron-density trace of the Shubnikov–de Haas oscillations in sample 4 at 0.35 K. The sudden decay of the amplitude of the oscillations is visible at ~1.5 T.

assign a filling factor of $\nu=2$ to the strong minimum.

For the highest densities (Fig. 4) a well developed set of SdH oscillations have appeared, and the low-field magnetoresistance has become much weaker. On closer inspection some unusual features of the oscillatory structure become apparent. First, there is a strong attenuation in the intensity of the oscillatory structure just below 2 T. Second, a plot of the positions of the SdH minima reveals they do not have a single constant period (Fig. 5). The plots show a clear break at approximately the field value where the intensity weakens, corresponding to the presence of two distinct electron densities in the structure. Specifically it should be noted that the periodicity decreases at higher fields, corresponding to a lower carrier density. This behavior is completely opposite to that seen in narrow wires,[14] where the 1D confinement leads to a decrease in period at low fields due to the confinement energy. Thus we have two different measures of the local carrier density in the structures. We choose the high-field, lower-density value (N_H) as the most convenient and widest-ranging measure, as it is readily measurable from the initial stages of the experiment. It is also somewhat closer to the value deduced from Hall measurements, which were only made extensively in the higher-density region due to contact resistivity problems in the more highly resistive state. Figure 6 shows a typical Hall trace in the most strongly patterned structure (sample 5) following full illumination. The field positions of the Hall plateaus are at approximately 10–30 % higher fields than the high-field resistivity minima, and are, in general, much more pronounced than the features seen in the resistivity. This indicates the high electron mobility in the conducting regions of the structure, as can also be judged by the appearance of a weak fractionally quantized feature at an occupancy of $\nu=\frac{4}{3}$ ($\rho_{xy}=19.4\ \Omega$), and may be related to differences in carrier density in different regions of the sample.

Figure 7 shows a plot of the zero-field conductivity as a function of carrier density (N_H). There is a rapid onset in conduction that occurs at progressively higher carrier densities as the patterning becomes stronger, when either the period is reduced or the implantation voltage is increased. This is accompanied by an increase in the magnitude of the low-field negative magnetoresistance, which is shown in Fig. 6 for a structure patterned at 42 keV. This large negative magnetoresistance is a particular feature of the strong patterning in our structures and has not generally been so strongly pronounced in reports by other workers.[5–7] The closest similarities are with the work of Ensslin and Petroff,[8] also on FIB-patterned structures where a clear negative magnetoresistance was also seen. At low carrier densities the zero-field conductivity of the array is often close to or below the quantum unit of conductivity $2e^2/h$, suggesting that the structure

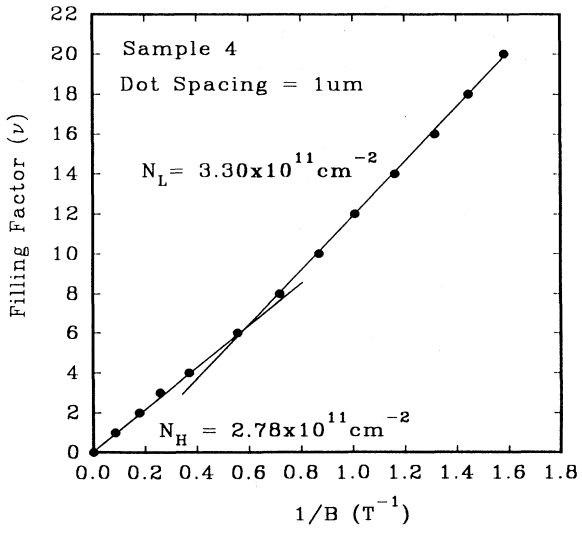

FIG. 5. $1/B$ plot of the positions of the conductivity minima showing the two different slopes and hence different carrier densities seen at low and high fields.

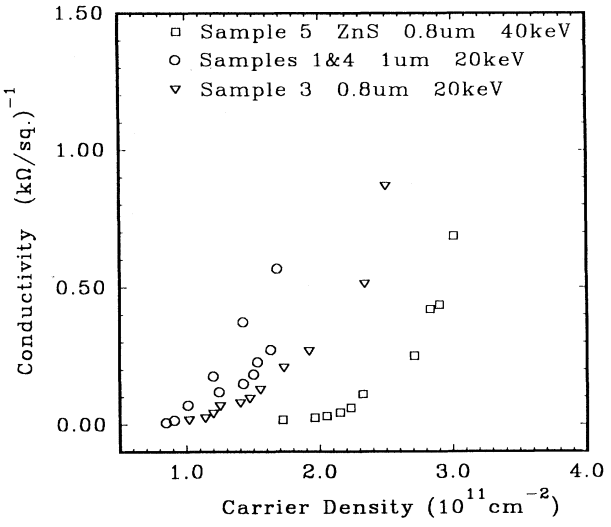

FIG. 6. The carrier-density dependence of the zero-field conductivity (at $T=0.6$ K for samples 1 and 3, $T=0.35$ K for samples 4 and 5) close to the onset of conduction. The carrier density N_H was determined from the high-field Shubnikov–de Haas oscillations. The solid lines show fits to Eq. (6), with the parameters shown.

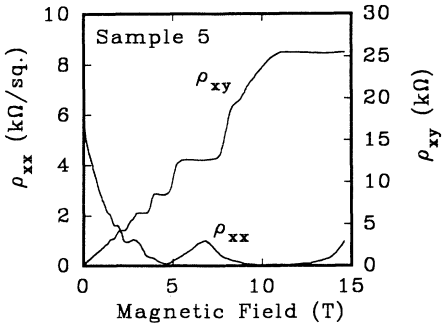

FIG. 7. The magnetoresistance and Hall voltage at 0.35 K for sample 5, showing the very large negative magnetoresistance for a strongly patterned structure.

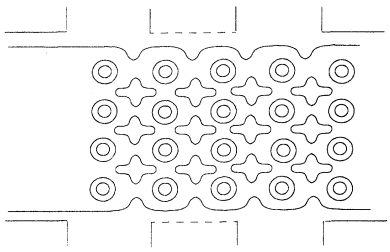

FIG. 8. A schematic picture of the electron orbits in high fields, showing how the propagating edge states are limited by the constrictions in the structure.

is behaving as an array of isolated point contacts. This is consistent with our estimates of the physical size of the constrictions (~ 0.3 μm long and ~ 0.1 μm wide), which are comparable to or smaller than those used in single point contact devices. In this regime the temperature dependence of the negative magnetoresistance (studied in detail in the accompanying paper[15]) is approximately linear, moving to an $\ln T$ dependence at higher carrier densities.

Finally it should be noted that we see no evidence of the resistivity peaks associated with pinball resonances recently reported by Weiss *et al.*[5] and Lorke, Kotthaus, and Ploog,[6] in which the carriers perform orbits pinned to sharp antidot potentials at a field corresponding to the commensurability of the classical orbit with the applied superlattice period. This in large part may be attributed to the fact that the physical geometry of the structures of Weiss *et al.*[5] and Lorke, Kotthaus, and Ploog[6] are such that they cannot be thought of as having a reservoir-constriction-reservoir geometry, but only as a periodic array of scattering centers.

IV. INTERPRETATION

The results indicate that the conductivity is very strongly carrier-density dependent. At low densities there is a strong localization of carriers in the dotlike reservoirs formed between the patterning array. The simultaneous observation of a very large negative magnetoresistance suggests that the carriers may be delocalized by the formation of edge states capable of propagating between adjacent dots. In the high-field limit these edge states become well formed and lose contact with the reservoirs (dots), thus causing a reduction in apparent carrier density.

This description is shown schematically in Fig. 8, where the propagating edge states can be seen to pass through the constriction regions between the adjacent dots, and correspond in the bulk of the structure to star-shaped orbits circling the depleted antidot array. By contrast, the orbits in the reservoir region correspond to closed circles formed from the higher Landau levels. Since the patterned regions extend beyond the edges of the Hall bar into the contact regions, these closed-reservoir orbits are not able to connect with the potential probes once the field is sufficiently large (>2 T) to form decoupled edge states. This will be true even in the presence of macroscopic disorder due to fluctuations in the ion-beam doping, since this occurs well beyond the 2DEG in the spacer layer. Consequently, only lower Fourier components of the scattering are present, which are not sufficient to mix different Landau levels (with $L_c \sim 150$ Å), which remain in the adiabatic limit. This is analogous to the mechanism proposed recently by Svobaoda *et al.*,[16] in which edge states in macroscopic Hall bars are decoupled from the localized states formed in the bulk. A similar explanation has been offered by van Wees *et al.*,[17] who showed that potential probes fabricated as point contacts to a macroscopic Hall bar could be used to make selective contact only to lower Landau levels.

At low fields the dot or reservoir regions become important once the edge-state description breaks down. The criterion for this is that the classical cyclotron orbit (R_c) at the Fermi energy exceeds the size of the smallest constriction (the neck) and the electrons are no longer able to propagate ballistically via the edge states.

$$R_c = \frac{V_F}{\omega_c} = \frac{\hbar\sqrt{2\pi N_s}}{eB} \ . \tag{1}$$

We estimate the constriction size to be of order 0.1 μm (in structures with periods of 0.8–1 μm), which corresponds to fields of 1–2 T using the cyclotron diameter. In this field range we observe the transition between the two types of behavior and hence the two-period SdH oscillations shown in Fig. 5. We are therefore able to identify the second low-field period with a measure of the carrier density (N_L) and hence the Fermi level in the dots. Within the framework of ballistic transport, at low fields there exists a high degree of backscattering that takes place within each reservoir when secular reflection takes place at the reservoir boundaries (leading to the high degree of localization, see Fig. 9). There is only a small probability of interdot communication that increases with the bending of the orbits by the magnetic field, until the field is high enough to induce skipping motion along the boundaries (edge states).

We can then plot the Fermi energies deduced from the carrier densities measured at high and low fields,

$$E_F = \frac{\pi N_s \hbar^2}{m^*} \ , \tag{2}$$

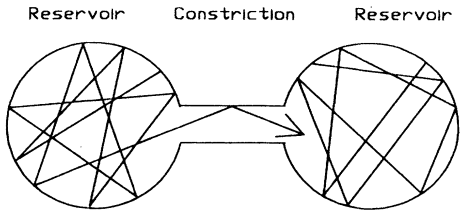

FIG. 9. A schematic picture of ballistic motion in two hard-walled reservoirs connected by a narrow constriction, showing the high degree of localization.

as a measure of the relative energies of the band edges in the reservoir (dot) and neck regions. This is shown in Fig. 10, where it can be seen that the structures are remarkably reproducible, and demonstrate a large modulation of the potential at low carrier densities, which is progressively screened out as the density increases. For weakly connected structures with only 1×10^{11} cm^{-2} carriers in the neck regions the modulation potential from reservoir to constriction is ~4 meV, but falls to ~1 meV by the time the neck region contains 3×10^{11} cm^{-2} carriers.

Finally, at very high magnetic fields we see a transition to a third, insulating state as the system reaches the quantum limit, as can be seen in the rapid rise in resistivity shown in Fig. 3. This occurs at a filling factor ≈1.5 for the lowest-density structures where the spin splitting is not resolved, and below $\nu\approx0.7$ for the higher densities.

$$\nu=\frac{N_s h}{2eB} . \tag{3}$$

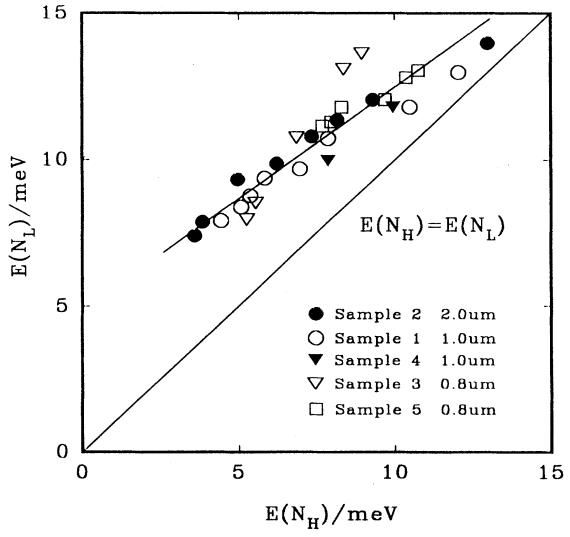

FIG. 10. A plot of the effective Fermi energies deduced from the low-field $E(N_L)$ and high-field $E(N_H)$ carrier concentrations. These correspond to the depths of the reservoir (dot) regions and the constriction (neck) regions.

The large increase in ρ_{xx} occurs as the edge states propagating via the neck regions become depopulated and all the carriers condense into the high degeneracy of the lowest Landau states centered on the reservoirs. In this case the system can undergo a classical metal-insulator transition associated with a percolation threshold as the interconnections via neck states are broken. This picture is quite similar to the behavior observed some time ago in low-mobility GaAs/Al_xGa_{1-x}As heterojunctions,[18,19] where similar rapid increases in the quantum limit magnetoresistance were observed. Again, the carriers were probably condensing into potential puddles which then became isolated from the current source and sink. In the quantum limit regime both the present and earlier results[19] also show that the resistivity becomes much more strongly temperature dependent, as conduction then proceeds via activation across neck barriers. No detailed analysis has yet been attempted.

It should be borne in mind that a classical percolation picture operating in high magnetic fields is in sharp contrast to the *low*-field behavior. Specifically, the observation of a large negative magnetoresistance and the formation of propagating edge states in high field suggests a quantum-mechanical view of localization at $B=0$ in which the partial transmission through individual constrictions is the dominating factor. A percolation view would be much more appropriate at high magnetic fields, where the individual bond (i.e., edge state) breaking will be discrete.

V. CONCLUSIONS

In summary, we find that strongly patterned antidot structures exhibit three distinct regions of differing magnetotransport properties: (i) low fields, in which the reservoirs are weakly interconnected and transport is dominated by the carrier density with each dot or reservoir leading to a strong negative magnetoresistance; (ii) high fields, in which propagating edge states are formed that penetrate the neck regions and become disconnected from the reservoirs; (iii) quantum limit, where the field is high enough to depopulate the propagating edge and neck orbits, and all the carriers condense into the reservoirs with no interconnections and a consequent percolation threshold.

The relative importance and field ranges of these phenomena can be modified by the strength and period of the modulating potential and the overall carrier density. The critical parameter is the size of the classical cyclotron orbit which determines the size of the ballistically propagating edge states. Our structures show behavior which is qualitatively different from that reported in earlier works on antidot arrays due to the much stronger nature of the patterning profile and the dominant role of the interconnects. The earlier works used structures in which the modulating potential was either weak in comparison to the Fermi energies of the underlying 2D electron gas[1-4] or had small repulsive cores[5,6] that allow ballistic propagation in orbits that avoid, but become pinned to, the addition potentials.

[1]D. Weiss, K. von Klitzing, K. Ploog, and G. Weimann, Europhys. Lett. **8**, 179 (1989).
[2]R. R. Gerhardts, D. Weiss, and K. von Klitzing, Phys. Rev. Lett. **62**, 1173 (1989).
[3]R. W. Winkler, J. P. Kotthaus, and K. Ploog, Phys. Rev. Lett. **62**, 1177 (1989).
[4]P. H. Beton, E. S. Alves, M. Hennini, L. Eaves, P. C. Main, O. H. Hughes, G. A. Toombs, S. P. Beaumont, and C. D. W. Wilkinson, J. Phys. Condens. Matter **1**, 8257 (1989).
[5]D. Weiss, M. L. Roukes, A. Menschig, P. Grambow, K. von Klitzing, and G. Weimann, Phys. Rev. Lett. **66**, 2790 (1991).
[6]A. Lorke, J. P. Kotthaus, and K. Ploog, Superlatt. Microstruct. **9**, 103 (1991).
[7]C. G. Smith, M. Pepper, R. Newbury, H. Ahmed, D. G. Hasko, D. C. Peacock, J. E. F. Frost, D. A. Ritchie, G. A. C. Jones, and G. Hill, J. Phys. Condens. Matter **2**, 3405 (1990).
[8]K. Ensslin and P. M. Petroff, Phys. Rev. B **41**, 12 307 (1990).
[9]G. M. Sundaram, N. J. Bassom, R. J. Nicholas, G. J. Rees, P. J. Heard, P. D. Prewett, J. E. F. Frost, G. A. C. Jones, D. C. Peacock, and D. A. Ritchie, in *Proceedings of the 20th International Conference on the Physics of Semiconductors, Thessaloniki, 1990,* edited by E. M. Anastassakis and J. D. Joannopoulos (World Scientific, Singapore, 1991), p. 2427.
[10]E. H. Linfield, D. A. Ritchie, G. A. C. Jones, J. E. F. Frost, and D. C. Peackock, Semicond. Sci. Technol. **5**, 385 (1990).
[11]Y. Hirayama, T. Saku, and Y. Horikoshi, Phys. Rev. B **39**, 5535 (1989).
[12]F. Laruelle, A. Bagchi, M. Tsuchiya, J. Merz, and P. M. Petroff, Appl. Phys. Lett. **56**, 1561 (1990).
[13]D. V. Morgan, in *Channeling* (Wiley, London, 1973).
[14]K. F. Berggen, T. J. Thornton, D. J. Newson, and M. Pepper, Phys. Rev. Lett. **56**, 1769 (1986).
[15]Y. Chen, R. J. Nicholas, G. M. Sundaram, P. J. Heard, P. D. Prewett, J. E. F. Frost, G. A. C. Jones, D. C. Peacock, and D. A. Ritchie, following paper, Phys. Rev. B **47**, 7354 (1993).
[16]P. Svoboda, P. Streda, G. Nachtwei, A. Jaeger, M. Cukr, and M. Laznicka, Phys. Rev. B **45**, 6390 (1992).
[17]B. J. van Wees, E. M. M. Willems, L. P. Kouwenhoven, C. J. P. M. Harmans, J. G. Williamson, C. T. Foxon, and J. J. Harris, Phys. Rev. B **39**, 8066 (1989).
[18]R. J. Nicholas, M. A. Brummel, and J. C. Portal. Surf. Sci. **113**, 290 (1982).
[19]M. A. Paalanen, D. C. Tsui, B. J. Lin, and A. C. Gossard, Surf. Sci. **142**, 29 (1984).